Solid State Communications 253 (2017) 42–45

Contents lists available at ScienceDirect

Solid State Communications

journal homepage: www.elsevier.com/locate/ssc

Communication

Topological crystalline insulator SnTe nanoribbons

Bishnu R. Dahal[a,b,*], Rajendra P. Dulal[a,b], Ian L. Pegg[a,b], John Philip[a,b]

[a] Department of physics, The Catholic University of America, Washington, DC 20064, Unites States
[b] The Vitreous State Laboratory, The Catholic University of America, Washington, DC 20064, United States

ARTICLE INFO

Keywords:
Nanoelectronics
Nanoribbons
Nanoscale device
Nanostructures
Semiconductor nanostructures
Topological insulator

ABSTRACT

Topological crystalline insulators are systems in which a band inversion that is protected by crystalline mirror symmetry gives rise to nontrivial topological surface states. SnTe is a topological crystalline insulator. It exhibits p-type conductivity due to Sn vacancies and Te antisites, which leads to high carrier density in the bulk. Thus growth of high quality SnTe is a prerequisite for understanding the topological crystalline insulating behavior. We have grown SnTe nanoribbons using a solution method. The width of the SnTe ribbons varies from 500 nm to 2 μm. They exhibit rock salt crystal structure with a lattice parameter of 6.32 Å. The solution method that we have adapted uses low temperature, so the Sn vacancies can be controlled. The solution grown SnTe nanoribbons exhibit strong semiconducting behavior with an activation energy of 240 meV. This activation energy matches with the calculated band gap for SnTe with a lattice parameter of 6.32 Å, which is higher than that reported for bulk SnTe. The higher activation energy makes the thermal excitation of bulk charges very difficult on the surface. As a result, the topological surfaces will be free from the disturbance caused by the thermal excitations

1. Introduction

Tin telluride is a group IV-VI semiconductor which crystallizes in rock salt crystal structure, and is reported to have a narrow direct band gap of 0.18 eV for bulk samples [1,2]. SnTe is an interesting material for several applications including infrared detector [3], thermoelectric generator [4], holographic recording [5], switching device [6], and for solar cell [7]. Recently, it was shown that SnTe can be classified based on topologies protected by point group symmetries of the crystal lattice. Those insulators that have nontrivial topology protected by point-group symmetries are called topological crystalline insulators (TCIs) [8]. So far concrete topological invariants are elucidated for systems possessing four-fold or six-fold rotation symmetry and also for systems with mirror symmetry. In particular, the latter case gained significant attention after the prediction that SnTe is a TCI [8]. Tanaka *et al.* experimentally confirmed the TCI behavior in SnTe; they observed surface state with the double Dirac cone structure [9]. SnTe is particularly unique as a platform to study valley-degenerate topological systems [10,11]. However, the growth of high-quality SnTe is a prerequisite to study such degeneracy effects and is also important for future devices based on TCI. Most of the growth techniques use high temperature that results in Sn vacancies and Te antisites which leads to p-type conductivity in SnTe. In case of thin films with small thicknesses, less than 1 μm, tend to be highly granular and rough, which can significantly reduce the carrier mobility [12–17].

We have grown two dimensional nanoribbons of SnTe having a high surface area using a solution method. Nanoscale devices were fabricated using e-beam lithography to understand the transport properties of these nanoribbons. Solution-grown SnTe nanoribbons exhibit a large bulk bandgap of 240 meV. Jin *et al.* have used a low temperature solution method to grow SnTe nanorods for solar cell application [18]. Shen *et al.* have grown SnTe nanoribbons and nanosheets using vapor-liquid-solid and vapor-solid mechanisms at a temperature of 873 K [10]. They have observed that the SnTe nanoribbons/sheets have higher bulk carrier density similar to that observed in bulk SnTe crystals.. In our synthesis, the maximum temperature used is 523 K and the growth is carried out without the use of catalyst, so the nanoribbons are free of chemical doping.

2. Experimental details

Nanoribbons of SnTe were synthesized using a two-step solution method. The first step of the synthesis was the growth of Te nanostructures, and the next step was to inject Sn precursor into the grown Te nanostructures to form SnTe nanoribbons. In a typical synthesis, 0.3*g* of high-purity polyvinylpyrrolidone was mixed with 0.24*g* of α-TeO_2 powder, followed by 20 ml of ethylene glycol along with 0.6 ml of hydrazine, and 0.6*g* of sodium hydroxide. The resulting solution was transferred to a three-necked flask fitted with a reflux

* Corresponding author at: Department of physics, The Catholic University of America, Washington, DC 20064, Unites States.
E-mail address: 62dahal@cua.edu (B.R. Dahal).

http://dx.doi.org/10.1016/j.ssc.2017.02.001
Received 12 September 2016; Received in revised form 31 January 2017; Accepted 2 February 2017
Available online 03 February 2017

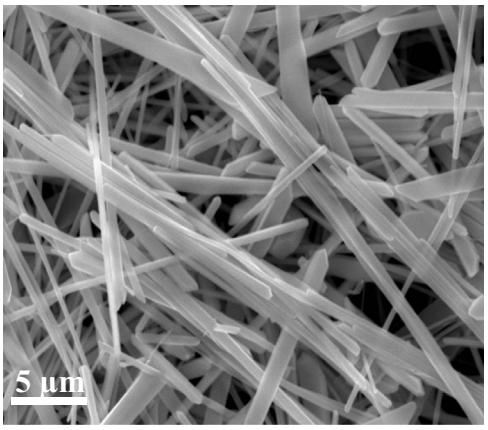

Fig. 1. Scanning electron microscopy image of SnTe nanoribbons.

condenser and a thermometer, and de-aerated by N_2 bubbling at 15cc/s. The solution in the flask was heated to a temperature of 433 K for 2 h, forming tellurium nanostructures and brought to room temperature. In the second step, required amount of $SnCl_2$ precursor was injected and then, raised the temperature to 523 K for 3 h. After cooling down to room temperature, the resultant solution was washed several times with ethanol, and acetone followed by centrifuge at 3000 revolutions per minute and finally dried at 373 K for 10 h in an argon environment. High quality SnTe nanoribbons are obtained only when the synthesis was carried out with TeO_2 and $SnCl_2$ as precursors for Te and Sn at 523 K. At lower temperatures, we have obtained multiple phases of Sn and Te nanoribbons and nanoparticles. We have initially carried out the synthesis with TeO_2 and SnO_2 as precursors, but have obtained both Sn deficient SnTe and Te nanowires, not nanoribbons. With SnO_2as a precursor for Sn, even with varied growth temperatures (453 – 523 K), SnTe nanoribbons were not formed. This low temperature synthesis method helps to reduce the Sn vacancies that are generally observed in high temperature growth techniques. The morphology of the nanoribbons was analyzed using a scanning electron microscope (SEM) (JEOL JSM-5410V); the crystal structure was determined by x-ray diffraction (XRD) (Thermo/ARL X'TRA, Cu-Kα) and transmission electron microscopy (TEM). Electrical transport properties were measured from a SnTe single nanoribbon device using a Quantum Design physical property measurement system.

3. Results and discussion

Fig. 1 shows the scanning electron microscopy image of SnTe nanoribbons. It clearly indicates the formation of nanoribbons with widths from 500 nm to 2 μm and lengths up to 50 μm. Fig. 2(a) shows the XRD pattern of SnTe nanoribbons. It exhibits rock salt (cubic, space group $Fm\bar{3}m$) crystal structure with a lattice parameter of 6.32 Å. Energy Dispersive X-ray (EDX) spectroscopy analyses were carried out on nanoribbons synthesized in three different batches. A typical spectrum is shown in Fig. 2(b). The EDX analyses show that the SnTe nanoribbons have Sn and Te at a 1:1 ratio. High-resolution transmission electron microscopy studies of these ribbons have shown that they are single crystalline. The lattice planes observed in Fig. 3(a) are (200) planes. Fig. 3(b) displays the selected area diffraction pattern of SnTe nanoribbons with the beam oriented along [110] direction. The diffraction spots are indexed using the rock crystal structure. Based on transmission electron microscopy analyses, nanoribbons with both $<111>$ and $<100>$ growth directions are observed. Nanoscale devices using ribbons were fabricated using the standard electron beam lithography technique to understand the electrical transport properties [19,20]. We have used Si (100) with a 500 nm of SiO_2 layer as substrates for device fabrication. Ohmic electrodes of thickness 150 nm [Ti(10 nm)/Au(140 nm)] were deposited using an ultra-high vacuum (base pressure 1×10^{-9} torr) deposition. The electrical transport measurements were carried out using two-probe method. Fig. 4(a) shows the typical current-voltage (I-V) characteristics of a single nanoribbon device at different temperatures. The I-V characteristics were measured from room temperature to 150 K. There is a 97% change in current flowing through the ribbons as the temperature is lowered from room temperature to 150 K at 1 V bias voltage. The nonlinear decrease in current with the decrease in temperature demonstrates that the SnTe nanoribbons display strong semiconducting behavior. The inset in Fig. 4(b) shows the SEM image of the device. Fig. 4(b) shows the temperature dependence of resistance from room temperature to 125 K measured with increasing temperature of the sample. The exponential decrease shown in the curve illustrates the semiconducting behavior of SnTe ribbons. Resistance of a semiconductor is related to the temperature as $ln(R) = ln(R_0)+E_a/k_BT$, where, R represents the resistance at temperature $T(K)$,R_0 represents resistance at 0 K, and k_B is the Boltzmann constant [21]. Fig. 4(c) is a plot of $ln(R)$ vs $1000/T$, which shows the expected linear behavior of a semiconductor. Activation energy, E_a can be calculated from the well fitted experimental data in Fig. 4(c) and the calculated activation energy is 240 meV. The observed activation energy matches with the calculated band gap value for SnTe with a lattice parameter 6.32 Å [8]. Hsieh *et al.* calculated the bandgap of SnTe as a function of lattice parameter, the band gap decreases with decrease in lattice parameter [8]. This E_a value observed in our ribbons is much greater than the value observed in common topological insulators like Bi_2Te_3 and Sn-doped Bi_2Te_2Se

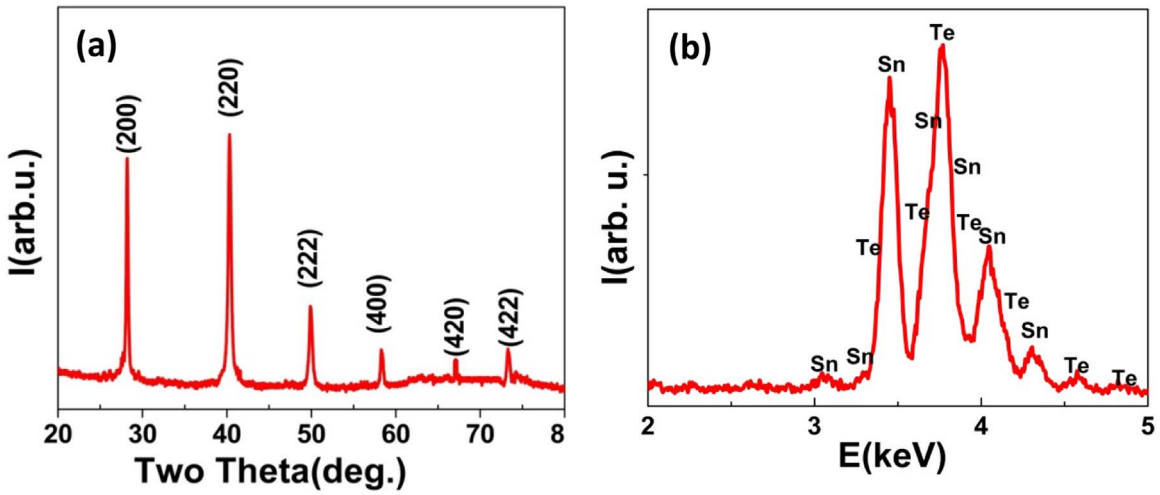

Fig. 2. (a) The XRD pattern and (b) the EDX spectrum of SnTe ribbons.

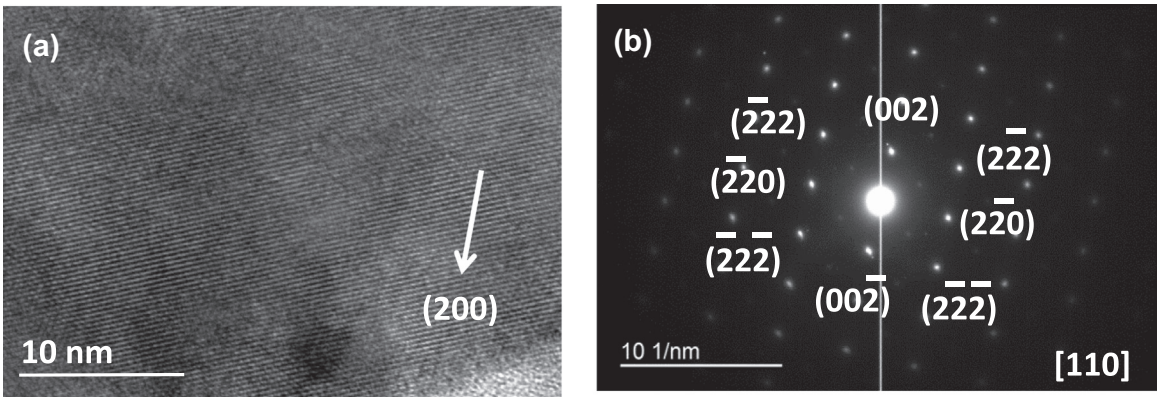

Fig. 3. (a) High resolution TEM image displaying the lattice fringes. (b) Selected area electron diffraction of SnTe single crystalline ribbons.

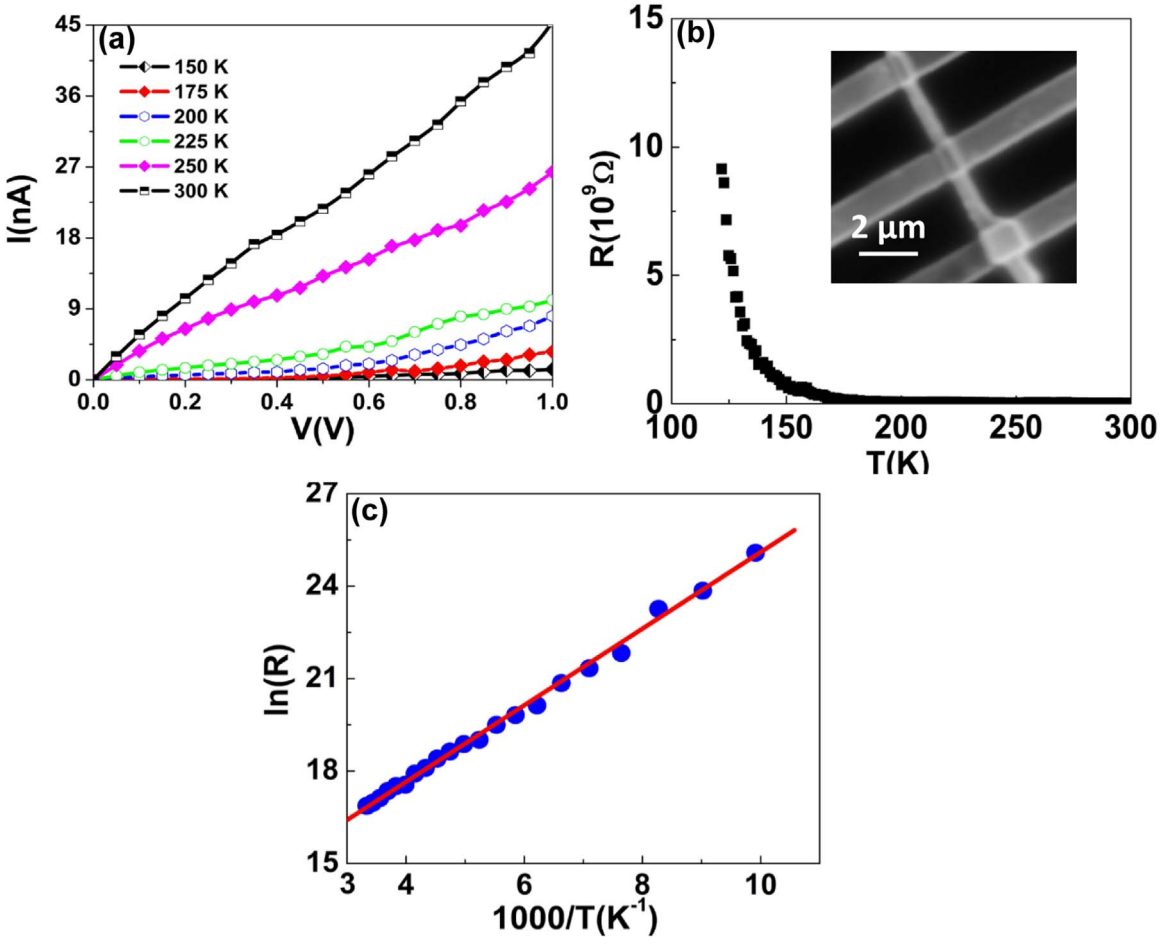

Fig. 4. (a) The current-voltage characteristics of the SnTe nanoribbon device. (b) Resistance as a function of temperature of a SnTe nanoribbon device. The inset shows the SEM image of the device and (c) the plot of lnR vs. 1/T displaying the linear characteristic of a semiconductor. The blue circles are experimental data and the line is a fit to the data.

having activation energy to be 2 meV and 125 meV respectively [22,23]. The higher activation energy makes the thermal excitation of bulk charges very difficult on the surface of the topological crystalline insulator.

4. Conclusions

Highly crystalline two dimensional SnTe nanoribbons were grown using a solution method. Nanoribbons display semiconducting behavior with an activation energy of 240 meV. These nanoribbons may exhibit better TCI behavior because of the strong bulk semiconducting behavior.

Acknowledgement

The authors thank Cathy Paul for carefully reading the manuscript.

References

[1] Y.W. Tung, M.L. Cohen, Phys. Rev. 180 (3) (1969) 823–826.
[2] J. Ning, K. Men, G. Xiao, B. Zou, L. Wang, Q. Dai, B. Liu, G. Zou, Cryst. Eng. Commun. 12 (2010) 4275–4279.
[3] C. Boschetti, I.N. Banderia, H. Closs, A.Y. Ueta, P.H.O. Rappl, P. Motisuke, E. Abramof, Infrared Phys. Technol. 42 (2) (2001) 91–99.
[4] G. Tan, L. –D. Zhao, F. Shi, J.W. Doak, S.-H. Lo, H. Sun, C. Wolverton, V.P. Dravid, C. Uher, M.G. Kanatzidis, J. Am. Chem. Soc. 136 (19) (2014) 7006–7017.
[5] R.K. Saini, R. Kumar, G. Jain, Optl. Mater. 32 (2) (2009) 297–301.

[6] K.A. Campbell, C.M. Anderson, Micro J. 38 (1) (2007) 52–59 (Jan. 2007).
[7] M.C. Beard, J.M. Luther, A.J. Nozik, Nat. Nanotechnol. 9 (2014) 951–954.
[8] T.H. Hesieh, H. Lin, J. Liu, W. Duan, A. Bansil, L. Fu, Nat. Commun. 3 (2012) 982.
[9] Y. Tanaka, T. Sato, K. Nakayama, S. Souma, T. Takahashi, Z. Ren, M. Novak, K. Segawa, Y. Ando, Phys. Rev. B 87 (15) (2013) 1–5.
[10] J. Shen, Y. Jung, A.S. Disa, F.J. Walker, C.H. Ahn, J.J. Cha, Nano Lett. 14 (7) (2014) 4183–4188.
[11] B.A. Assaf, F. Katmis, P. Wei, B. Satpati, Z. Zhang, S.P. Bennett, V.G. Harris, J.S. Moodera, D. Heiman, Appl. Phys. Lett. 105 (2014) 102108.
[12] A.P. Bakhtinov, V.N. Vodop'yanov, V.I. Ivanov, Z.K. Kovalyuk, O.S. Lytvyn, Phys. Sol. Stat. 55 (2013) 181–195.
[13] A. Ishida, T. Yamada, T. Tsuchiya, Y. Inoue, S. Takaoka, T. Kita, Appl. Phys. Lett. 95 (2009) 122106.
[14] S.O. Ferreira, E. Abramof, P.H.O. Rappl, A.Y. Ueta, H. Closs, C. Boschetti, P. Motisuke, I.N. Bandeira, J. Appl. Phys. 84 (1998) 3650.
[15] E. Abramof, S.O. Ferreira, P.H.O. Rappl, H. Closs, I.N. Bandeira, J. Appl. Phys. 8 (1997) 2405–2410.
[16] U.A. Mengui, E. Abramof, P.H.O. Rappl, A.Y. Ueta, Braz, J. Phys. 26 (2006) 324–327.
[17] A.A. Taskin, F. Yang, S. Sasaki, K. Segawa, Y. Ando, Phys. Rev. B 89 (2014) 121302.
[18] H.D. Jin, C.-H. Chang, J. Mater. Chem. 21 (2011) 12218.
[19] B.R. Dahal, R.P. Dulal, I.L. Pegg, J. Philip, J. Vac. Sci. Technol. 34 (2016) 051801.
[20] B.R. Dahal, R.P. Dulal, I.L. Pegg, J. Philip, Mater. Res. Express 3 (2016) 116101.
[21] X. Wang, Z. Xie, H. Huang, Z. Liu, D. Chen, G. Shen, J. Mater. Chem. 22 (2012) 6845–6850.
[22] S. Cho, N.P. Butch, J. Paglione, M.S. Fuhrer, Nano Lett. 11 (2011) 1925–1927.
[23] Z. Ren, A.A. Taskin, S. Sasaki, K. Segawa, Y. Ando, Rev. B 85 (15) (2012) 155301.